Ray theory of flow instability and the formation of caustics in boundary layers

Benoit-Joseph Gréa [1], Paolo Luchini [2], Alessandro Bottaro [3]
[1] *IMFT, Allée du Prof. C. Soula, 31400 Toulouse, France*
[2] *Dipartimento di Ingegneria Meccanica, Università di Salerno, 84084 Fisciano, Italy*
[3] *DIAM, Università di Genova, via Montallegro 1, 16145 Genova, Italy*

The propagation of waves in an inhomogeneous medium, or of small disturbances in a fluid flow, is often cumbersome to study, even by numerical means, because of the presence of fast oscillations. On the other hand, when the oscillations become fast enough, both of these phenomena lend themselves to a geometrical approximation using ray theory. A ray, formally defined as a characteristic line of the eikonal equation, may be considered as a path along which the main contribution to the Green's function propagates. When dealing with instability waves in nonparallel boundary layers, the ray coordinates are complex-valued. The extension to the complex plane of techniques which are standard for the propagation of conservative waves can lead to useful asymptotic methods approximating the instability, as will be shown in the example of the Falkner-Skan-Cooke flow. In this approach, singularities may arise when multiple rays become tangent at a point, leading to the formation of a caustic. The existence of caustics in boundary layers is demonstrated and a method is proposed to account for their presence.

PACS: 47.20-k, 47.35.+i, 42.25.-p

I. INTRODUCTION

The prediction of instabilities leading to transition in three-dimensional boundary layers has been the subject of intense research over the last thirty years. Since transition in most shear flows is influenced to a great extent by environmental conditions, it is of great interest to be able to determine the spatial development of disturbances induced by a small external forcing. This may be alternatively characterized in time by an impulse response or by the response to harmonic forcing. Both problems constitute canonical models, whose understanding is indispensable to develop predictive tools to appraise the stability characteristics and the ensuing transition phenomenon for, *e.g.*, the flow over swept wings. Depending on the physical situation one model may be more pertinent than the other: a small roughness element on a wing, for example, might be modelled as a harmonic forcing of zero frequency, whereas the injection of atmospheric turbulence into the boundary layer is best represented as an impulse forcing. Since it is typically very difficult to assess properly the receptivity environment which determines transition under a wide range of conditions, each one of these two configurations deserves particular attention.

When the disturbances are of small amplitude, a numerical solution of the linearized Navier-Stokes equations is in principle possible. In practice, however, whereas such a numerical solution is viable for slowly-varying disturbances (transient growth), a rapidly oscillating Tollmien-Schlichting wave in a Blasius boundary layer undergoes at least 50 (spatial) periods of oscillation in its amplification towards transition. To properly capture the instability over a long region of space, a very refined grid is needed, rendering the numerics very costly, particularly when a detailed parametric study is required.

A more elegant and computationally efficient approach can be traced back to early work by [1], who solved the linearized Navier-Stokes equations for the impulse-response problem in a parallel flow using asymptotic methods, focussing on the most amplified mode. Gaster obtained the wave packet by writing the disturbance in the form of a double integral in the spectral domain, which he evaluated by a steepest descent method. For each given direction of propagation, a saddle point in spectral space was identified, point which provides the largest contribution to the integral. This procedure introduces the concept of ray in hydrodynamic stability, defined as the line along which the instability wave propagates. In a seminal article [2] applied the concept of *kinematic wave theory* (see [3] and [4]) to flow instability within the problem of shear-flow transition. In particular, Landahl used the concept of rays which are the characteristic lines of the dispersion relation for the wave vector. The extension of the theory, originally developed for neutral (or quasi-neutral) waves, to instability waves is not straightforward. The generalization to the case of unstable waves was apparently initiated by [5]. He solved the linearized Navier-Stokes equations subject to a point-wise impulse forcing by performing a multiple-scale analysis. The leading-order problem yields the eikonal equation which Itoh treated by the method of characteristics, leading to ray theory.

In parallel flows, there is perfect equivalence between ray theory and the Fourier-integral formulation of, for example, [1]. With time, a number of improvements over the original integral formulation were proposed. For example, around the most amplified wavenumber, which plays a crucial role in transition, an expansion can be made to compute the disturbance, leading to the *gaussian* approximation proposed by [6]. On the other hand, the many different studies on convective/absolute instabilities which appeared in the literature in the last thirty years encouraged people in the way of using the original approach, *i.e.* to pursue a solution of the impulse and/or

harmonic forcing problems by closing the contour of integration and using the residue theorem to apply Briggs' method. [7] provides an example and a complete way to compute three-dimensional wave packets in parallel flows.

Whereas the integral formulation is perfectly appropriate for parallel flows, problems arise when trying to handle an inhomogeneous base motion, such as that occurring over a swept tapered wing, because a Fourier transform can no longer be applied. Here, ray theory shows its full power. In weakly non-parallel flows the inhomogeneities produce curved rays which, when the growth rate of the instability differs from zero, force the ray trajectories to go into the complex plane. This has been the crux of the problem for some time. Initially, a number of attempts were made to force the rays to remain in the real plane, but it was proved later that this *real axis approximation* can be grossly inaccurate (see [8]).

We also note that more than one definition has been provided in weakly non-parallel flows of the amplification undergone by an instability wave. To compute the N-factor used to identify the transition "point" by the e^N method, one has to integrate the amplification rate along the path followed by the energy-transporting wave. This path is determined by the group velocity, i.e. by the rays. [9], for example, developed a theory (denoted as the "zarf") that yields the N-factor by conducting the integration over the locus of points with real group velocity. Whereas this approach provides a conservative estimate of the maximum amplification, because as will be shown later the amplification rate is greatest when wavenumber and group velocity are simultaneously real, it actually compounds together amplification rates that belong to different waves, and thus does not accurately represent any one of them. For this latter purpose it is necessary to use the local properties of the flow and compute the complex-valued trajectory of each instability wave in coordinate-wavenumber space [40]. One of the first applications of complex-ray theory to boundary layers was performed by [10]. He found the disturbance at a given physical point in a Falker-Skan-Cooke boundary layer (model of the flow over an infinite swept wing) by computing the ray which starts from a point source and reaches a target point through a path in complex space. [11] used a similar method and also underlined the confusion thereto made in e^N methods as applied to non-parallel flows. A complete mathematical formulation of complex-ray theory as applied to fluid mechanics has recently been developed by [12]. Much earlier applications have existed, of course, in fields such as electromagnetics, quantum mechanics, plasma dynamics and laser optics (see *e.g.* [13]).

The approach we will present here is similar to Itoh's and Lingwood's, but we bring some extra theoretical results concerning the *physical optics* approximation, *i.e.* the subsequent correction to the leading-order approximation (known as *geometrical optics*) and concerning the possible appearance of *caustics* in the pattern of rays. Furthermore, in [5] the treatment of the compatibility condition was approximated; here a method is developed to exactly handle this condition. Finally, the fact that rays transport both the phase and the amplitude of the disturbance is shown. Through examples, we shall also examine where and when it is important to account for the *physical optics* correction.

We choose to focus on wedge-shaped disturbances originating from a harmonic point source in a Falker-Skan-Cooke flow. Whereas this example is of some practical interest (since it is an intermediate step towards the swept wing) it is interesting also in that it demonstrates the existence of caustics in a boundary layer. The phenomenon of caustics is very well known in other fields of physics; for fluid flows it is known to take place, for example, on the edges of the wake produced by a boat progressing in still water. In this problem, the boat can be modeled by a steady point source, and it can be shown that an interaction between waves propagating in the direction toward and away from the boat lead to this effect ([14]). On the other hand, impulse forcing in time would correspond here to a stone thrown in a river: the circular wave crests cannot self-interact and no caustics are found. In boundary layers, the word caustic first appeared in [1] and then in [15] for a time-impulsive excitation (see also [16]). In [11]'s reconsideration of the impulse problem no caustics were found. However, the question remains open on whether caustics can indeed occur in the propagation of flow instabilities, because the case of time-harmonic forcing has not yet been considered. This case is addressed here on some specific (representative) test problems, issued from a general theoretical background.

II. COMPLEX-RAY THEORY

To develop the mathematical formulation of complex-ray theory as applied to instability waves in weakly inhomogeneous media we start from classical multiple-scale analysis, following the lead of authors such as [17], [18], [19] and [20]. The theory of characteristics is then applied to the eikonal equation, obtained from the leading-order equations.

A. Multiple-scale analysis in boundary layers

We consider the conventional dimensionless Navier-Stokes equations for an incompressible fluid whose state

[40] The formulation of the problem may lead to rays with either complex coordinates or complex wavenumber or both.

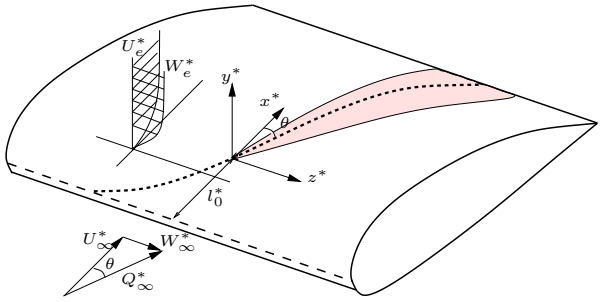

FIG. 1: Boundary layer development over an infinite swept wing. The attachment line is shown as a dashed line; the external streamline is plotted with dotted line and the velocity profiles in the reference frame attached to the chordwise direction is also sketched.

is defined by a velocity vector $\mathbf{V}$ and a pressure field P:

$$\begin{aligned} \frac{D\mathbf{V}}{Dt} &= -\nabla P + \frac{1}{Re}\nabla^2\mathbf{V}, \\ \nabla\cdot\mathbf{V} &= 0. \end{aligned} \tag{1}$$

The coordinate system is defined by x^*, streamwise coordinate, y^*, wall-normal coordinate and z^*, spanwise coordinate, a superscript $*$ referring to dimensional quantities. In the system of equations (1), D/Dt denotes the convective derivative, and the Reynolds number is defined as:

$$Re = \frac{Q_e^*\delta^*}{\nu}, \tag{2}$$

with $Q_e^* = \sqrt{(U_e^*)^2 + (W_e^*)^2}$, U_e^* being the x^*-component of the velocity outside the boundary layer, W_e^* the z^* component of the velocity outside the boundary layer and δ^* being a representative boundary-layer thickness (which in the particular case of Falkner-Skan-Cooke flow will be taken $\delta^* = (l_0^*\nu/Q_e^*)^{\frac{1}{2}}$, in terms of the abscissa l_0^* where the disturbance is applied, *cf.* figure 1). Thus, all lengths are nondimensionalized by δ^*, velocities by Q_e^* and time by δ^*/Q_e^*. The system is closed by no-slip boundary conditions at the solid wall and by the imposed free-stream conditions.

The state of the system is decomposed into a steady base flow plus a small disturbance:

$$\begin{aligned} \mathbf{V} &= \overline{\mathbf{V}} + \mathbf{v}, \\ P &= \overline{P} + p. \end{aligned} \tag{3}$$

We then apply the boundary layer approximation. A small parameter ϵ is introduced, function of the ratio of the characteristic transverse to the longitudinal scale; it indicates the property of the boundary layer that variations along the directions x and z are slower than along the direction normal to the wall y. New coordinates are then introduced, defined by $X = \epsilon x$, $Y = y$, $Z = \epsilon z$ and $T = \epsilon t$, so that the base flow can be written as a power series in ϵ:

$$\begin{aligned} \overline{\mathbf{V}}(x,y,z) &= \mathbf{V}_0(X,Y,Z) + \mathbf{V}_1(X,Y,Z)\epsilon + ... \\ \overline{P}(x,y,z) &= P_0(X,Y,Z) + P_1(X,Y,Z)\epsilon + ... \end{aligned} \tag{4}$$

Upon inserting (4) into system (1), the leading-order term in the continuity equation trivially yields $V_0 = 0$.

B. Linear system for the disturbance

The disturbance equations are obtained by substituting (3) into system (1). Quadratic terms for the disturbances are neglected and only a time harmonic frequency ω is considered. This leads to the following linear system:

$$\begin{aligned} -i\omega u + \epsilon\overline{U}u_X + \overline{V}u_Y + \epsilon\overline{W}u_Z + \epsilon u\overline{U}_X + v\overline{U}_Y + \epsilon w\overline{U}_Z \\ = -\epsilon p_X + \frac{1}{Re}\left(\epsilon^2 u_{XX} + u_{YY} + \epsilon^2 u_{ZZ}\right) \end{aligned}$$

$$\begin{aligned} -i\omega v + \epsilon\overline{U}v_X + \overline{V}v_Y + \epsilon\overline{W}v_Z + \epsilon u\overline{V}_X + v\overline{V}_Y + \epsilon w\overline{V}_Z \\ = -\epsilon p_Y + \frac{1}{Re}\left(\epsilon^2 v_{XX} + v_{YY} + \epsilon^2 v_{ZZ}\right) \end{aligned}$$

$$\begin{aligned} -i\omega w + \epsilon\overline{U}w_X + \overline{V}w_Y + \epsilon\overline{W}w_Z + \epsilon u\overline{W}_X + v\overline{W}_Y + \epsilon w\overline{W}_Z \\ = -\epsilon p_Z + \frac{1}{Re}\left(\epsilon^2 w_{XX} + w_{YY} + \epsilon^2 w_{ZZ}\right) \end{aligned}$$

$$\epsilon u_X + v_Y + \epsilon w_Z = 0 \tag{5}$$

As already mentioned, we observe that in its general formulation ray theory can handle the case of impulse forcing in time (*cf.* [5] and [11]).

C. Multiple-scale (WKB) analysis

To solve the linear system (5) two procedures are possible. The first approach, based on an asymptotic expansion in which ϵ, Re^{-1} and ω are simultaneously driven to zero in a coupled manner, leads to a multiple-deck formulation. The wall-normal direction is decomposed into several layers, the number of which changes with the assumed asymptotic dependence between ω and Re, and the solution is expressed in the form of matched asymptotic expansions. The advantage of this method is that an explicit dependence on the parameters is obtained, in the form of a power series. However, when practical applications are sought after, *i.e* when the Reynold number is not exceedingly large, the convergence of this method is slow and the leading-order term of the series does not provide a sufficiently accurate solution. Another method, yielding a solution uniformly valid in y, consists of asymptotically expanding equations (5) with respect to ϵ only, while retaining their exact parametric dependence

on ω and Re. This is, without doubt, formally allowed, even in cases in which the value of ϵ we are finally interested in is $O(Re^{-1})$ (see *e.g* [21]). *Not* neglecting higher-order terms in Re^{-1} and ω does not harm the accuracy of the solution. In addition it should be noted that the limit of $\epsilon \to 0$ for fixed ω and Re is physically realizable, for instance in a channel with slowly diverging walls or in a boundary layer subject to a steady external bulk force. The appropriate expansion in the limit of $\epsilon \to 0$ for given ω and Re is the multi-dimensional equivalent of a WKB expansion (see, for example, [1] and [19]).

We thus look for solutions of (5) in the form:

$$\begin{aligned} \mathbf{v}(X,Y,Z) = &\quad e^{i\frac{\Phi(X,Z)}{\epsilon}}\left(\mathbf{v}_0(X,Y,Z) + \mathbf{v}_1(X,Y,Z)\epsilon + ...\right), \\ p(X,Y,Z) = &\quad e^{i\frac{\Phi(X,Z)}{\epsilon}}\left(p_0(X,Y,Z) + p_1(X,Y,Z)\epsilon + ...\right). \end{aligned} \tag{6}$$

The disturbance is represented as a wave rapidly oscillating in the X and Z directions, and thus having a large phase Φ/ϵ.

The local wavenumbers of the disturbance can be defined as:

$$\begin{aligned} \alpha = &\quad \frac{\partial \Phi}{\partial X}, \\ \beta = &\quad \frac{\partial \Phi}{\partial Z}. \end{aligned} \tag{7}$$

To obtain equations of successive orders for the disturbance, we substitute (6) into (5), and make use of (4). Thence:

- Order ϵ^0:

$$\begin{aligned} i(\alpha U_0 + \beta W_0 - \omega)u_0 + U_{0Y}v_0 \\ = -i\alpha p_0 + \frac{1}{Re}\left(u_{0YY} - (\alpha^2+\beta^2)u_0\right) \\ i(\alpha U_0 + \beta W_0 - \omega)v_0 \\ = -p_{0Y} + \frac{1}{Re}\left(v_{0YY} - (\alpha^2+\beta^2)v_0\right) \\ i(\alpha U_0 + \beta W_0 - \omega)w_0 + W_{0Y}v_0 \\ = -i\beta p_0 + \frac{1}{Re}\left(w_{0YY} - (\alpha^2+\beta^2)w_0\right) \\ i\alpha u_0 + v_{0Y} + i\beta v_0 = 0 \end{aligned} \tag{8}$$

- Order ϵ^1:

$$\begin{aligned} i(\alpha U_0 + \beta W_0 - \omega)u_1 + U_{0Y}v_1 = \\ -i\alpha p_1 + \frac{1}{Re}\left(u_{1YY} - (\alpha^2+\beta^2)u_1\right) + A_1, \\ i(\alpha U_0 + \beta W_0 - \omega)v_1 = \\ -p_{1Y} + \frac{1}{Re}\left(v_{1YY} - (\alpha^2+\beta^2)v_1\right) + A_2, \\ i(\alpha U_0 + \beta W_0 - \omega)w_1 + W_{0Y}v_1 = \\ -i\beta p_1 + \frac{1}{Re}\left(w_{1YY} - (\alpha^2+\beta^2)w_1\right) + A_3, \\ i\alpha u_1 + v_{1Y} + i\beta v_1 = A_4, \end{aligned} \tag{9}$$

with A_1 to A_4 given in Appendix A. In this paper we do not address the limit in which ϵ and Re^{-1} (and possibly ω) simultaneously tend to zero. In such a limit slightly different forms of equations (8-9) can be introduced which differ in their asymptotic error estimation but often produce practically equivalent results, see *e.g* [22] and [23].

D. Local eigenvalue problem

In order for the solution $(\mathbf{v}_0, p_0)$ of system (8) to exist, the wavenumbers α, β and the frequency ω have to satisfy a dispersion relation which we formally write as:

$$F(\alpha, \beta, \omega, X, Z) = \quad 0. \tag{10}$$

Equation (10) can alternatively be made explicit with respect to one of its arguments. It is straightforward to show that (8) can be reduced to the following Orr-Sommerfeld/Squire eigenproblem:

$$\begin{aligned} [(-i\omega + i\alpha U_0 + i\beta W_0)(\mathcal{D}^2 - k^2) - i\alpha U_{0YY} \\ -i\beta W_{0YY} - \frac{1}{Re}(\mathcal{D}^2 - k^2)^2]v_0 = 0, \\ [(-i\omega + i\alpha U_0 + i\beta W_0) - \frac{1}{Re}(\mathcal{D}^2 - k^2)]\eta_0 \\ = \left[i\alpha W_{0Y} - i\beta U_{0Y}\right] v_0, \end{aligned} \tag{11}$$

with $\eta_0 = i(\beta u_0 - \alpha w_0)$, $k = \alpha^2 + \beta^2$ and $\mathcal{D}$ denoting derivation with respect to Y. The boundary conditions for this system are:

$$\begin{aligned} v_0 = \mathcal{D}v_0 = 0 \text{ at} \quad Y = 0 \text{ and } Y \to +\infty, \\ \eta_0 = 0 \text{ at} \quad Y = 0 \text{ and } Y \to +\infty. \end{aligned} \tag{12}$$

The above equations have been solved by a pseudospectral collocation technique, implemented in MatLab. We have chosen to discretize the Y direction at the Gauss-Lobatto points, with at least 30 collocation points inside

the boundary layer. A shooting method is used to solve the spatial eigenvalue problem for the mode of interest.

Since we only look for the most amplified streamwise wavenumber, it is convenient to express (10) as:

$$\alpha = f(\beta, \omega, X, Z) \tag{13}$$

α denoting the numerically determined eigenvalue from the above procedure.

E. The equations for the rays

The local properties defined by the dispersion relation (13) are all that is needed to determine the global propagation of the instability. In fact, the phase Φ can now be computed as the solution to the eikonal equation, defined as the equation that is obtained after sustituting (7) into (13):

$$\Phi_X = f(\Phi_Z, \omega, X, Z). \tag{14}$$

This first-order partial differential equation for Φ can be solved by the method of characteristics, as explained, *e.g.*, in [24] (p. 75). This yields the equations for the rays:

$$\begin{aligned} \frac{dZ}{dX} &= -\frac{\partial \alpha}{\partial \beta}, \\ \frac{d\beta}{dX} &= \frac{\partial \alpha}{\partial Z}, \\ \frac{d\Phi}{dX} &= \alpha - \beta \frac{\partial \alpha}{\partial \beta}, \end{aligned} \tag{15}$$

X having been chosen as the variable which parameterizes the rays.

The first equation of system (15) gives the trajectory of a ray in the (X, Z) plane. The slope of this trajectory in space is determined by a "group direction" $d_g = -\partial\alpha/\partial\beta$, which is *a priori* a complex number. This is the main difference with standard ray theory developed for nondissipative waves by *e.g.* [14]. The possible occurrence of unstable waves implies that the physical Z space is complex, *i.e.* a ray is a curve in the three-dimensional space (X, Z_r, Z_i) (subscripts r and i referring to the real and imaginary part of the variable). The second of equations (15) yields the variation of the spanwise wavenumber β, and the last equation provides the spatial variation of the phase itself along the ray.

The choice of X as the independent variable is motivated by the fact that the base flow depends on this coordinate, which is thus kept real. With this choice we avoid having to perform an analytical continuation of the base flow in complex space. On the other hand, when the base flow also depends on Z (as is the case for the motion over swept tapered wings), the analytic continuation cannot be avoided.

The ray equations can be solved numerically by computing at each position X the dispersion relation and its derivatives; the spatial integration of equations (15) is performed here with a fourth-order Runge-Kutta scheme. In the examples presented later, 10 streamwise points have proven sufficient to ensure the convergence of the ray trajectories.

F. Action principle for the rays

In this section an alternative formulation of ray theory is outlined, classical for purely dispersive waves but whose extension to complex rays is not widely known; it provides a complementary view and some useful properties for the rest of the work. The ray equations can be rewritten in the following form:

$$\begin{aligned} \frac{dZ}{dX} &= \frac{\partial H}{\partial \beta}, \\ \frac{d\beta}{dX} &= -\frac{\partial H}{\partial Z}, \end{aligned} \tag{16}$$

with $H = -\alpha$. As indicated by [4], [14] and many others before, equations (16) describe a Hamilton system with H the Hamiltonian; X plays the role of time, Z that of position and β is the *momentum*.

It is then possible to derive an action principle. A Lagrangian operator associated to H can be defined as:

$$L = \beta \frac{dZ}{dX} - H. \tag{17}$$

The *action* associated to an arbitrary path in the X-Z plane can be expressed as the integral:

$$S = \int_{X_1}^{X_2} L dX, \tag{18}$$

which is a function of the path of integration and of the initial and final stations X_1 and X_2. Incidentally, we note that we could also have defined an ordinary "temporal Lagrangian", leading to the same action as an integral over time rather than X, had we aimed at solving the problem of the impulse response, like [5] or [11].

As explained for instance in [25], it is possible to show the equivalence between (16) and the fact that the action is an extremum if the path of integration is the ray. This principle is widely used in optics to define the ray, *i.e.* the shortest *optical path* (Snell's law), as well as in classical and in quantum mechanics. The main difference here is that the functions S, H and L are complex-valued and defined for complex arguments (see [13] on the subject). Nonetheless we still find, comparing (18) and the last of (15), that the value of the action integral computed *along the ray* equals the (complex) phase difference between the final and initial state:

$$S(X_1, Z_1, X_2, Z_2) = \Phi_2 - \Phi_1. \tag{19}$$

A ray can be specified either by its starting coordinates and wavenumber or by its initial and final positions

(X_1, Z_1) and (X_2, Z_2), in the same way as in classical mechanics the trajectory of a particle is determined either by its initial position and momentum or by two positions at different instants of time. The action (phase difference) associated with the ray that passes through given initial and final positions has useful properties. When Z_1 or Z_2 are modified, following [25] (p. 205), it is possible to write:

$$\frac{\partial S(X_1, Z_1, X_2, Z_2)}{\partial Z_1} = -\beta_1 \; ; \; \frac{\partial S(X_1, Z_1, X_2, Z_2)}{\partial Z_2} = \beta_2. \tag{20}$$

This property depends only on formal differentiation of the integral (18), and remains true in the complex domain. Sometimes, it is preferable to specify a ray with its final position Z_2 and initial *momentum* β_1. The change of variables from Z_1 to β_1 corresponds to a *canonical* transformation of the action into

$$\hat{S}(X_1, \beta_1, X_2, Z_2) = S(X_1, Z_1, X_2, Z_2) + \beta_1 Z_1. \tag{21}$$

Differentiating this function with respect to β_1 and using (20) yields a useful formula that we shall exploit later:

$$\frac{\partial \hat{S}(X_1, \beta_1, X_2, Z_2)}{\partial \beta_1} = Z_1. \tag{22}$$

It is important to observe that all the intermediate steps leading to (22), although classically presented for conservative systems only, remain valid when the action and its arguments are complex.

G. Propagation of a sinusoidal disturbance along rays

Let us suppose that at the initial station X_1, for a given forcing of temporal frequency ω, we have a disturbance sinusoidal in the Z-direction of amplitude $\mathcal{A}$ and large wavenumber β_1/ϵ. It is possible to write it in the form:

$$\mathbf{a}(X_1, Z_1, Y) = \mathcal{A}(X_1, Z_1)\hat{\mathbf{a}}_0(X_1, Z_1, Y)e^{i\frac{\beta_1 Z_1}{\epsilon}} \tag{23}$$

In the above expression, $\hat{\mathbf{a}}_0 = (\hat{\mathbf{v}}_0, \hat{p}_0)$ denotes the normalized eigenfunction of the most amplified mode computed at the position X_1. The normalization is performed so that the maximum modulus of v_0 equals 1 for every X, Z. By considering only the most amplified eigenfunction, we suppose that the disturbance will be dominated by this mode at X_2, far enough from X_1. This is generally verified for Tollmien-Schlichting modes. For every specified physical mechanism which creates the excitation, the initial amplitude $\mathcal{A}$ at X_1 can be obtained from the *receptivity* coefficient for the disturbance through a suitable adjoint calculation (see, for example, [26] and [27]). For the present purposes, $\mathcal{A}$ is considered to be a given (slowly varying) function of Z_1 and the problem consists in computing the propagation of an initial sinusoidal disturbance, using ray theory, up to a specified final location (X_2, Z_2). *A fortiori*, these coordinates are real since we are interested in the physical effect of the disturbance, but the intermediate path of each ray is allowed to be complex. Only the leading order of the WKB expansion, $\mathbf{a}_0$, is initially considered. It is represented as the product of the vector normalized eigenfunction $\hat{\mathbf{a}}_0$ and the scalar amplitude $\mathcal{A}$. The perturbation produced at X_2 can then be written as follows:

$$\mathbf{a}(X_2, Z_2, Y) = \mathcal{A}(X_2, Z_2)\hat{\mathbf{a}}_0(X_2, Z_2, Y)e^{\frac{i}{\epsilon}\Phi_2(X_2, Z_2)} \tag{24}$$

The phase Φ_2 is associated with the ray of initial *momentum* β_1 at station X_1 passing through the point (X_2, Z_2), and can be calculated from the last of equations (15), *i.e.* from the integral of the Lagrangian (17), with the initial condition $\Phi_1 = \beta_1 Z_1$. As the initial condition has a narrowly determined wavenumber but an infinite range of Z, the departure position Z_1 of this ray is *a priori* undetermined, and may turn out to be complex. The determination of Z_1 is considerably simplified if it is observed that $\Phi_2(X_2, Z_2)$ coincides with the action $\hat{S}(X_1, \beta_1, X_2, Z_2)$ as defined in equation (21), so that property (22) applies to it. The wavenumber β_2 is derived from the second of the ray equations (15), or alternatively as $\partial\hat{S}/\partial Z_2$, and equals β_1 if the base flow is homogeneous in the Z-direction. The amplitude $\mathcal{A}$ can also be obtained along each ray, by the procedure that is detailed next.

H. Propagation of the amplitude

In order to compute the amplitude $\mathcal{A}$ it is necessary to write a compatibility condition using the $\mathrm{O}(\epsilon)$ equations (9). We start by rewriting (8) and (9) in compact form, as:

$$\begin{aligned} \mathbf{L}(\mathbf{a}_0) &= 0, \\ \mathbf{L}(\mathbf{a}_1) &= \chi(\mathbf{a}_0), \end{aligned} \tag{25}$$

with $\chi = (A_1, A_2, A_3, A_4)$. We now introduce the scalar product

$$< \mathbf{b}, \mathbf{a} > = \int_0^{+\infty} \mathbf{b}^+ \mathbf{a} \; dY, \tag{26}$$

with the symbol $^+$ denoting conjugate transpose. From (25) the following compatibility condition is found:

$$< \hat{\mathbf{b}}_0, \chi(\mathbf{a}_0) > = \; 0, \tag{27}$$

with $\hat{\mathbf{b}}_0$ the normalized eigenfunction of the operator adjoint to $\mathbf{L}$.

In (27) $\mathbf{a}_0$ is now replaced by $\mathcal{A}\hat{\mathbf{a}}_0$ and, using the expression for χ, we obtain the first-order scalar differential equation:

$$< \hat{\mathbf{b}}_0, \gamma_{\mathbf{X}} > \mathcal{A}_X + < \hat{\mathbf{b}}_0, \gamma_{\mathbf{Z}} > \mathcal{A}_Z + < \hat{\mathbf{b}}_0, \gamma_{\mathbf{0}} > \mathcal{A} = \; 0, \tag{28}$$

where the vectors $\gamma_{\mathbf{X}}, \gamma_{\mathbf{Z}}$ and $\gamma_{\mathbf{0}}$ are given in Appendix B. The above equation for $\mathcal{A}$ can be solved by the method of characteristics (just as the eikonal equation (14)). The slope of the characteristics for this linear first-order partial differential equation in the (X, Z) plane is given by $- < \hat{\mathbf{b}}_0, \gamma_{\mathbf{Z}} > / < \hat{\mathbf{b}}_0, \gamma_{\mathbf{X}} >$.

It is interesting to note that (even when Z is complex-valued) the characteristics of the amplitude equation (28) are just the rays. At a given station (X, Z), we can differentiate the leading-order equation (25) with respect to β. This gives:

$$\mathbf{L}_\beta(\beta,\alpha)\mathbf{a}_0(\beta) + \frac{\partial\alpha}{\partial\beta}\mathbf{L}_\alpha(\beta,\alpha) + \mathbf{L}(\beta,\alpha)\mathbf{a}_{0\beta}(\beta) = \quad 0. \tag{29}$$

By taking the scalar product of (29) with the adjoint eigenfunction $\hat{\mathbf{b}}_0$ and using the properties of the adjoint we obtain the following result (already shown by [28]):

$$\frac{\partial\alpha}{\partial\beta} = -\frac{< \hat{\mathbf{b}}_0, \mathbf{L}_\beta \mathbf{a}_0 >}{< \hat{\mathbf{b}}_0, \mathbf{L}_\alpha \mathbf{a}_0 >}. \tag{30}$$

It is possible to check directly that $-i\mathbf{L}_\alpha = \gamma_{\mathbf{X}}$ and $-i\mathbf{L}_\beta = \gamma_{\mathbf{Z}}$. This proves the result that the rays are also the characteristic lines of the equation for the amplitude, even in complex Z. We show in Appendix C that this is a general property of this kind of systems. As a consequence, the rays are the trajectories followed by the instability, *i.e.* they transport both the phase and the amplitude of the wave.

It is then possible to solve (28) and obtain:

$$\mathcal{A}(X_2, Z_2) = \mathcal{A}(X_1, Z_1) e^{-\int_{X_1}^{X_2} \frac{<\hat{\mathbf{b}}_0, \gamma_{\mathbf{0}}>}{<\hat{\mathbf{b}}_0, \gamma_{\mathbf{X}}>}\, dX}, \tag{31}$$

where the integral in (31) is carried out along the path followed by the ray.

It is also important to observe that whereas the value of $\mathcal{A}$ depends on the normalization of the egeinfunction $\hat{\mathbf{a}}_0$, the product $\mathbf{a}_0 = \mathcal{A}\hat{\mathbf{a}}_0$, being the solution of the WKB system (25), is independent of this arbitrary choice.

I. Propagation of an initially pointlike disturbance

When the disturbance at the initial station X_1 is not a wave packet, *i.e* cannot be locally approximated by a sinusoid, then indirect methods must be adopted to study its propagation. This is particularly true for the case of a disturbance concentrated at a single position $Z = 0$; a single ray is not sufficient to get a correct approximation of the disturbance wavepacket downstream. On the other hand, if the pointlike disturbance is expanded in a Fourier representation, the solution can be written as an integral in spectral space. With the receptivity coefficient (*i.e.* the initial amplitude) previously computed and its Fourier transform denoted as $\hat{\mathcal{A}}(X_1, \beta_1)$, the initially localised disturbance can be written as:

$$\mathbf{a}(X_1, Z_1, Y) = \int_{-\infty}^{+\infty} \hat{\mathcal{A}}(X_1; \beta_1)\hat{\mathbf{a}}_0(X_1, Z_1, Y; \beta_1) e^{i\frac{\beta_1 Z_1}{\epsilon}} d\beta_1, \tag{32}$$

i.e. as a sum of sinusoidal disturbances. The propagation of the disturbance to the point (X_2, Z_2) can be calculated from (24) (also denoted as a Maslov integral, see [29]):

$$\mathbf{a}(X_2, Z_2, Y) = \int_{-\infty}^{+\infty} \mathcal{A}(X_2, Z_2; \beta_1)\hat{\mathbf{a}}_0(X_2, Z_2, Y; \beta_1) e^{\frac{i}{\epsilon}\Phi_2(X_2, Z_2)} d\beta_1. \tag{33}$$

In $\hat{\mathbf{a}}_0$ we have explicitely indicated β_1 as a parameter. It is clear, however, that the calculation of $\hat{\mathbf{a}}_0$ in (33) is performed by entering β_2 in the local eigenvalue problem (11), with β_2 related to β_1 through the second of equations (15).

To compute (33) without having to compute a ray for every value of β_1, a steepest-descent method can be used (see *e.g.* [30]). In this method, the saddle point $\beta^\star$ of the phase $\Phi_2(X_2, Z_2) = \hat{S}(X_1, \beta_1, X_2, Z_2)$ provides the main contributions to the integral. Such a point is defined by:

$$\frac{\partial \hat{S}}{\partial \beta_1}(X_1, \beta^\star, X_2, Z_2) = 0. \tag{34}$$

In the case of a pointlike disturbance, from (22), we obtain that the ray corresponding to the saddle point starts from $Z_1 = 0$, consistently with the idea that the initial disturbance is concentrated at this point. In the case of a parallel flow, when $\beta_2 = \beta_1$, to find the position $\beta^\star$ of the saddle point one has to solve the following problem by iterative methods (see [10]):

$$Z_2 = -\int_{X_1}^{X_2} \frac{\partial\alpha}{\partial\beta} dX \tag{35}$$

The saddle-point approximation of the disturbance at a given location is then:

$$\mathbf{a}(X_2, Z_2, Y) \simeq \mathcal{A}(X_2, Z_2; \beta^\star)\hat{\mathbf{a}}_0(X_2, Z_2, Y; \beta^\star) e^{\frac{i}{\epsilon}\hat{S}(X_1, \beta^\star, X_2, Z_2)} \sqrt{\frac{2\pi i\epsilon}{\frac{\partial^2 \hat{S}}{\partial \beta_1^2}\,|_{\beta^\star}}}, \tag{36}$$

the accuracy of the result being of the same order as that of the WKB approximation.

J. Falkner-Skan-Cooke equations for the base flow

A frequently used model for the flow over a swept wing is the family of similarity solutions for yawed wedge flows

developed by [31]. It introduces two parameters: m, related to the pressure gradient, and θ, which is the angle between the external velocity components. We follow the classical method to compute the base flow described in [32], using the similarity variable $\xi = (U_e^*/(\nu x^*))^{1/2} y^*$. The flow outside the boundary layer is supposed to behave like $U_e^* = C(x^*)^m$ and W_e^* =constant. Upon posing $\overline{U}^* = U_e^* f'(\xi)$ and $\overline{W}^* = W_e^* g(\xi)$ the functions f and g are found to satisfy:

$$\begin{aligned} f''' + \frac{m+1}{2} f f'' + m(1 - f'^2) = &\quad 0, \\ g'' + \frac{m+1}{2} f g' = &\quad 0, \end{aligned} \tag{37}$$

with

$$f(0) = f'(0) = g(0) = 0 \; and \quad f'(\infty) = g(\infty) = 1, \tag{38}$$

$\overline{U}^*$ and $\overline{W}^*$ are obtained by solving numerically the system (37). The velocity normal to the wall $\overline{V}^*$ is then deduced from mass conservation. When the Falkner-Skan-Cooke flow is used as a local approximation of a more general three-dimensional boundary layer, U_e^* and W_e^* are taken as the local external velocity components and m is deduced from the local velocity gradient as $m = ({x_{eq}}^*/U_e^*)\partial U_e^*/\partial x^*$, where x_{eq} is not the actual abscissa along the surface but the equivalent position at which an exact Falkner-Skan-Cooke boundary layer along a wedge would have the same momentum thickness.

III. APPLICATION OF RAY THEORY TO PARALLEL FLOWS

A. Determination of the complex saddle points

In order to test the accuracy of the steepest-descent approximation to compute the disturbance originating from a spatially localized time-harmonic source, we start from the study of a parallel base flow. In this context, the local dispersion relationship (13) does not depend on X and Z. As a consequence, α, β and the slope $\frac{\partial \alpha}{\partial \beta}$ of a ray are constant and we drop the suffix $_1$ and $_2$ in the expressions for them. A ray with a given initial β passing through a given point (X_2, Z_2) has then to satisfy:

$$Z_2 = -\frac{\partial \alpha}{\partial \beta}(X_2 - X_1) + Z_1, \tag{39}$$

and the corresponding phase, using (15) reads:

$$\Phi_2 = \alpha (X_2 - X_1) - \frac{\partial \alpha}{\partial \beta} \beta (X_2 - X_1) + \Phi_1, \tag{40}$$

Thus the above expression (40) can be simplified using (39) and the fact that $\Phi_1 = \beta Z_1$ to read:

$$\Phi_2 = \alpha(X_2 - X_1) + \beta Z_2. \tag{41}$$

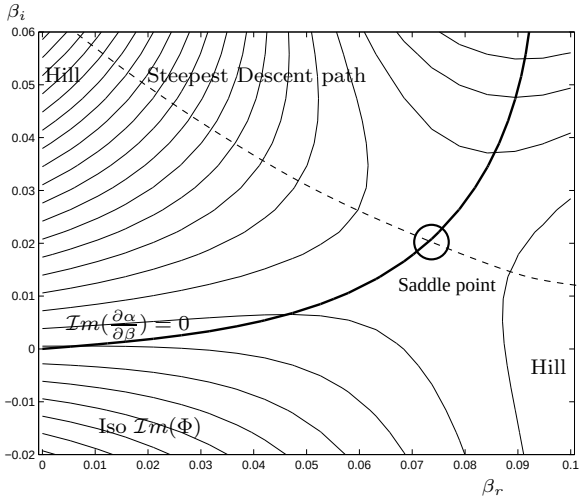

FIG. 2: Steepest descent path for a parallel Blasius flow with $Re = 1000, \omega = 0.04$ and for the ray $\frac{Z}{X} = 0.15$. Also plotted with thick line is the path where the group direction $d_g = -\frac{\partial \alpha}{\partial \beta}$ is real. This path is the locus of the different saddle points when the direction $\frac{Z}{X}$ is changed.

By differentiating (41) with respect to β and imposing the saddle point condition (34), it is easy to check the relation $Z_1(\beta^\star) = 0$, *i.e* the ray giving the main contribution starts from the position where the perturbation originates. All this is, of course, consistent with the fact that for a parallel base flow the WKB approximation becomes coincident with the exact solution $\Phi = \alpha X + \beta Z$.

For Z_2, X_1 and X_2 to be real, the condition (39) gives that the group direction d_g must be real at the saddle point while the chordwise wavenumber $\beta^\star$ associated to it is generally complex. As discussed in [33] and [34] (but for the group velocity in a temporal representation), the very fact that the saddle-point condition (39) identifies $\partial\alpha/\partial\beta$ as the slope of the straight line connecting (X_1, Z_1) to (X_2, Z_2) leads us to denote this quantity as the *group direction* d_g (up to a minus sign). We thus see that in the parallel case d_g is always real whereas β^* can be complex [40].

The rays associated with saddle points are straight lines starting from the origin of the perturbation in the real plane X, Z. The locus of the $\beta^\star$ associated to each ray direction can be represented in the complex plane, as the curve where $\partial\alpha/\partial\beta$ is real. Figure 2 gives an example, for Blasius flow, of such a curve in the complex-β plane. The steepest-descent path and the iso-contours of the imaginary part of Φ_2 are also represented, for a single value of d_g, for later use.

The ray (or direction) which has the biggest amplification plays a crucial role as it may indicate where the instability triggers the transition process. Therefore, we outline a procedure to find it easily in our representation. The amplification can be calculated from the imaginary part of $\Phi_2(X_2, Z_2) = \hat{S}(X_1, \beta^\star, X_2, Z_2)$ and is a maxi-

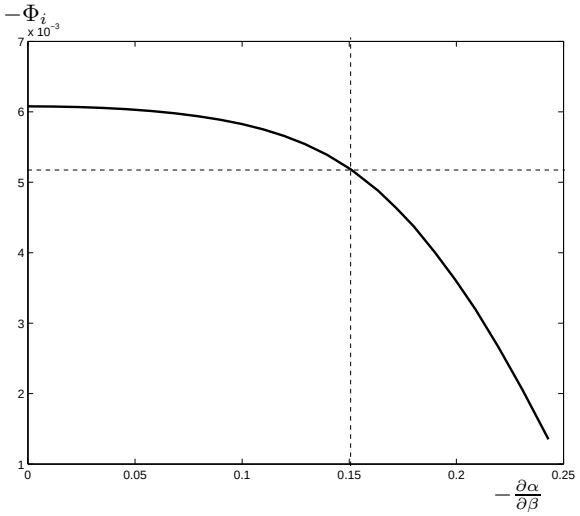

FIG. 3: Amplification rate ($-\mathcal{I}m(\Phi)$) as a function of the group direction, along the branch where the group direction is real for the ray $\frac{Z}{X} = 0.15$ corresponding to the saddle point on figure 2, $\Phi_i = -0.0052$. Blasius base flow with $Re = 1000, \omega = 0.04$.

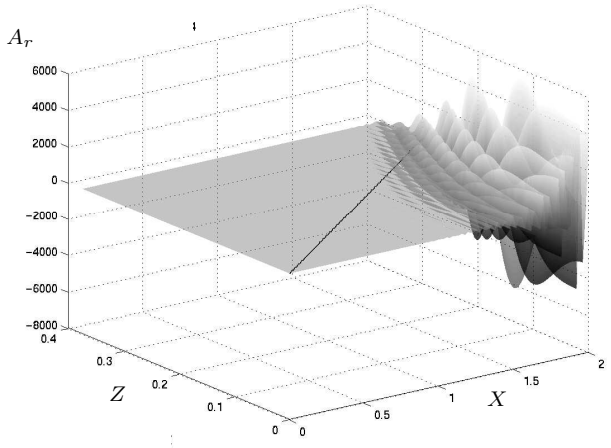

FIG. 4: Wedge-shaped disturbance in a parallel Blasius flow at $Re = 1000$ and $\omega = 0.04$. The straight line is the ray $\frac{Z}{X} = 0.15$.

mum when $d\mathcal{I}m(\hat{S})/dZ_2 = 0$; the differentiation gives:

$$\frac{d\hat{S}}{dZ_2} = \frac{\partial\hat{S}}{\partial Z_2} + \frac{\partial\hat{S}}{\partial\beta^\star}\frac{d\beta^\star}{dZ_2} \tag{42}$$

but, since $\partial\hat{S}/\partial\beta^\star = 0$ by definition of $\beta^\star$,

$$\frac{d\hat{S}}{dZ_2} = \frac{\partial\hat{S}}{\partial Z_2} = \beta_2 \tag{43}$$

Hence, the amplification is the largest at the position Z_2 where β_2 is real. In the parallel case, when $\beta_2 = \beta_1 = \beta^\star$, we have $\mathrm{Im}(\beta^\star) = 0$ as the condition for the maximum amplification rate (see also [1] or [35] for the analogous demonstration in the temporal case). In figure 2, the intersection of the locus of the saddle points with the real axis is at $\beta^\star = 0$ ($d_g = 0$) and the corresponding maximum can be seen on the curve for the amplification rate in figure 3.

The maximum is not always situated at the origin of the β-plane. In the example considered later in figure 11, the locus of the saddle points meets the real axis at $\beta^\star \neq 0$.

B. Accuracy of ray theory

Since our asymptotic method to compute disturbances is an approximation, we need to check that it gives accurate enough results in areas of parameter space where the growth rate of the unstable mode becomes significant. In parallel flows the integral (33) actually represents the exact solution of the problems, and can be computed by numerical quadrature to any desired accuracy. Such computations have been performed with a very fine integration step for different wave configurations in parallel Blasius flow, and compared to the saddle-point approximation of the same integral. On choosing, in particular, an initial disturbance represented by a δ-function in Z_1, and therefore by a constant in β, the amplitude A at X_2 will be expressed by

$$A(X_2, Z_2) = \int_{-\infty}^{+\infty} e^{\frac{i}{\epsilon}[\alpha(\beta_1)X_2 + \beta_1 Z_2]} d\beta_1. \tag{44}$$

Figure 4 shows the real part of this amplitude to take the form of a wedge-shaped disturbance. The value of β yielding the maximum amplification is 0, corresponding to the case studied in figure 2 and 3. In figure 5, on the other hand, a case for which the β of largest amplification is different from zero is displayed. Both cases refer to a Reynolds number of 1000. In both figures the amplitude of the instability is observed to grow exponentially from the origin $(0, 0)$, and to produce a wedge-shaped disturbance packet which becomes of visible amplitude on the scale of the plot near the exit section only ($X = 2$).

At the fixed position $X = 2$ a comparison is made between the exact amplitude provided by the inverse transform and its saddle-point approximation; as shown in figures 6 and 7 the agreement is good. On the other hand, in the case of figure 8 where the β of maximum amplification is non zero, the amplitude A is not caught very well by the first order approximation of the integral (44). To explain this behaviour and obtain a better estimate of A, we must evaluate differently the integral, upgrading the steepest descent approximation. This technique, referred to as Airy approximation, will prove very useful in the handling of singularities, such as caustics.

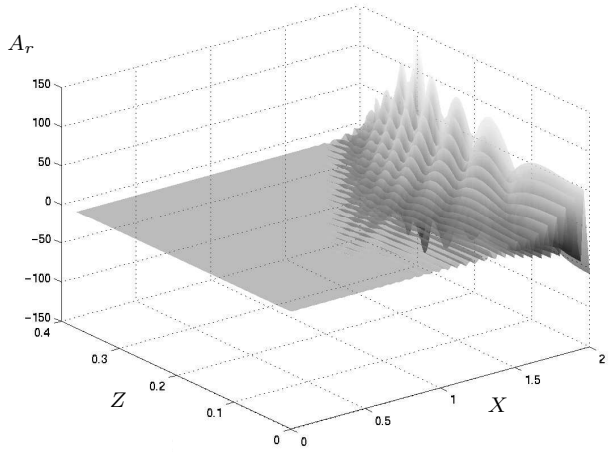

FIG. 5: Wedge-shaped disturbance in a parallel Blasius flow at $Re = 1000, \omega = 0.03$.

IV. CAUSTICS

A. Occurrence of caustics

By reducing the forcing frequency from $\omega = 0.03$ to $\omega = 0.025$ we encounter a case worthy of discussion. Figure 9 shows the "exact" real part of the amplitude of the disturbance in a case where the β of maximum amplification is clearly different from 0 and the wave packet excited at $(X_1, Z_1) = (0, 0)$ propagates laterally. The comparison with ray theory is provided at $X_2 = 4$ in figure 10. It can be noticed that the agreement is good everywhere except in a neighbourhood of $Z_2 = 0.68$, where standard steepest descent yields visibly larger amplitude values. This divergence is due to the fact that the term $\frac{\partial^2 \Phi_2}{\partial \beta_1^2}$ in equation (36) approaches zero.

To properly appraise this phenomenon, we have plotted isolines of the imaginary part of the phase Φ in figure 11, for two different rays in the complex β plane; such isolines are the steepest-descent paths. The first observation is that the line of real $d_g = -\partial\alpha/\partial\beta = Z_2/X_2$ has two branches, named I and II here. Thus, two cases can be encountered. For large angles, or large values of Z_2/X_2 (figure 11 a), the steepest-descent path goes through one saddle point only, like in figure 2. Ray theory produces then a good agreement with the direct computation. For smaller Z_2/X_2, however, two saddle points occur (marked by bold circles in figure 11b). Generally, one saddle point provides a much larger contribution to the integral than the other, since it has a larger amplification rate; in this case it is sufficient to consider only its contribution. This occurs in this example for $\frac{Z_2}{X_2} = 0.2$ so that ray theory is in good agreement with the direct computation of the integral (33). It is not the case, however, when the two saddle points happen to give comparable amplification rates, so that both have to be considered.

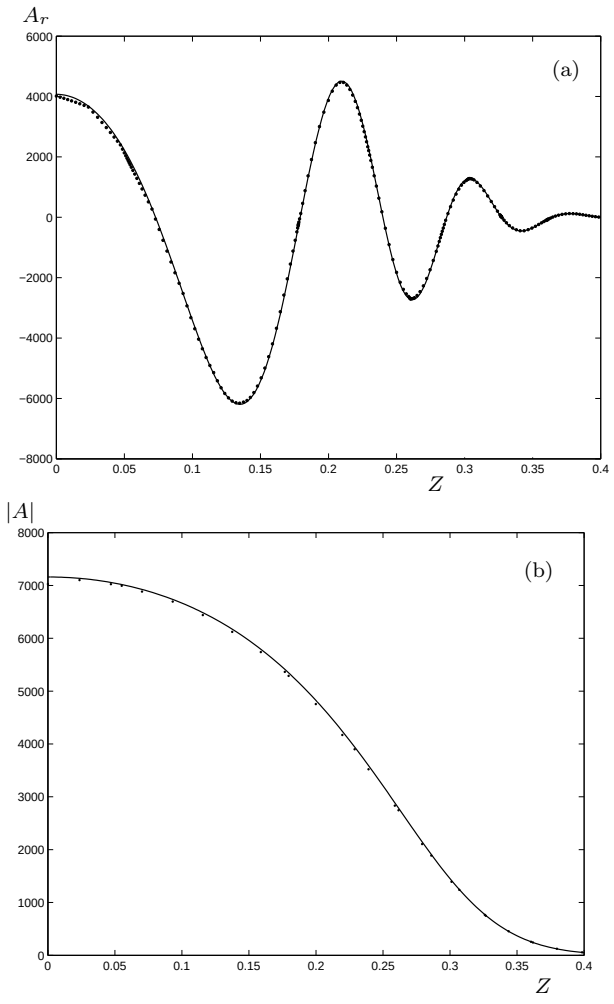

FIG. 6: Comparison of real part (a) and absolute value (b) of the integral for A. (–) is the direct computation and (.) is ray theory. Parallel Blasius flow at $Re = 1000, \omega = 0.04$ at $X = 2$.

To identify where this occurs we have plotted in figure 12 the growth factor on each branch as a function of the group direction. The bifurcation between one saddle point and two saddle points on the steepest descent path occurs at a point $\mathcal{C}$ in the complex-β plane where the second derivative $\frac{\partial^2 \alpha}{\partial \beta^2}$ equals zero (*cf.* figure 11). In figure 12, branch II is shown as a dashed line beyond the complex caustic point $\mathcal{C}$, where it does not provide anymore a contribution to the integral (33), despite the fact that its amplification rate is larger than that provided by branch I.

However, close to the complex caustics point $\mathcal{C}$ the growth rates of the two branches are of the same order, and both must be accounted for in the evaluation of the disturbance amplitude, *i.e* a single ray is unable to yield a correct estimate of the instability wave.

This phenomenon is even more important if it occurs close to the most amplified direction. As shown earlier

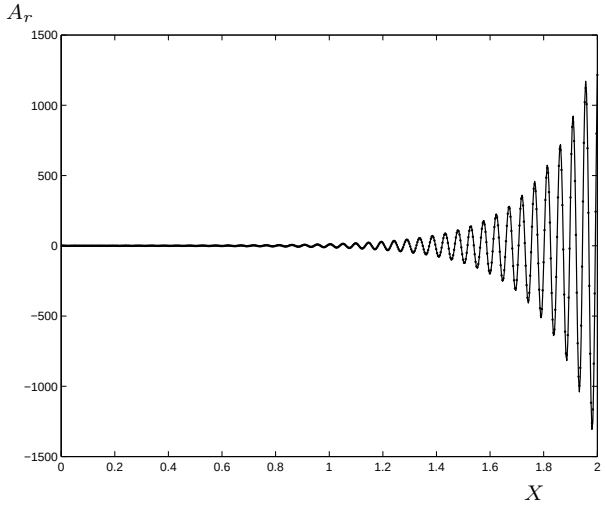

FIG. 7: Comparison of direct computation of the integral (44) and ray theory for a parallel Blasius flow at $Re = 1000, \omega = 0.04$ on the ray $\frac{Z}{X} = 0.15$. Symbols as in figure 6.

in this paper, the value of β associated to the most amplified direction is real, so that it can be identified in the graphs as the direction where one branch intersects the real axis. The example we have just shown is one in which the caustic is very close to the direction of maximum amplification (*cf.* figure 12).

A mathematical analogy can be observed with the behavior identified by Healey [38] in studying the large-Reynolds asymptotics of absolute instabilities of the rotating-disk boundary layer. He found that the second derivative $\partial^2\omega/\partial\alpha^2$ was vanishing at the same time as the first for a complex α and a certain combination of real β and Re, and termed it as a *super branch point*. The caustic as traditionally encountered in optics arises during the spatial propagation of a time-harmonic wave field, and this is the case that we deal with in this paper; however, if β takes the role of frequency and time the role of spatial direction of propagation, Healey's problem is obtained. In this sense, his *super branch point* of absolute instabilities might also be seen as a time-like caustic. Both his case and ours are characterized by divergence of the saddle-point approximation of the wave field, and in both this divergence can be corrected by considering higher-order terms in the Taylor series of the exponent.

B. Higher-order approximation of the disturbance wave

To compute wave amplitudes around caustics, we refer to techniques well known in optics (see *e.g* [36]). In this section we will provide a higher-order approximation of (33), by deforming the contour of integration to the steepest descent path $\mathcal{P}$ and using a Taylor-series expansion in β_1 around the saddle point to approximate

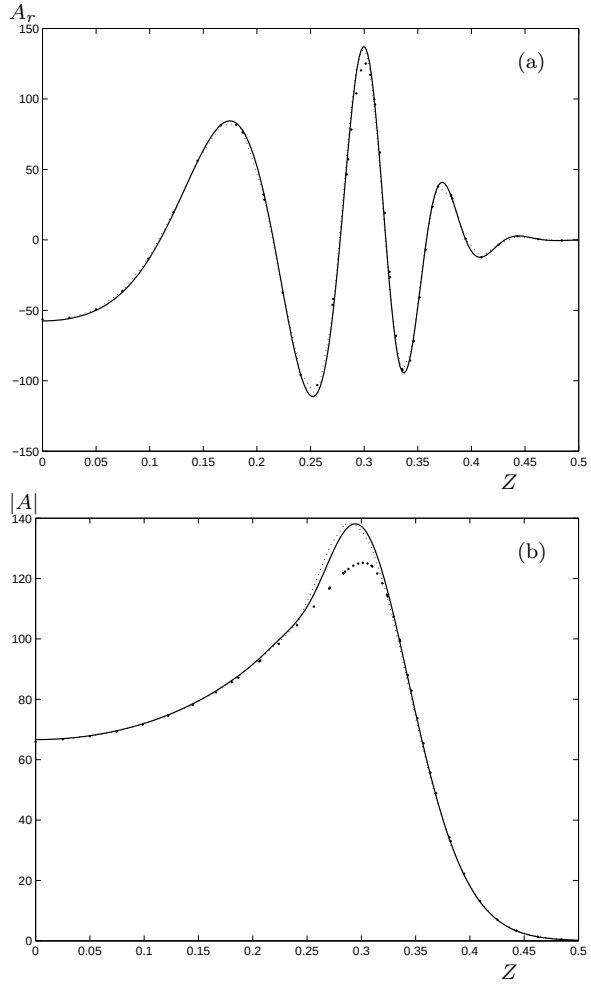

FIG. 8: Comparison of real part (a) and absolute value (b) of the integral (44). (—) is the direct computation, $(\cdot)$ is ray theory and the dotted line (...) is the approximation of A based on Airy functions. Parallel Blasius flow at $Re = 1000, \omega = 0.03$ at $X = 2$.

the phase:

$$\mathbf{a}_{int} \simeq \int_{\mathcal{P}} \mathcal{A}\hat{\mathbf{a}}_0 e^{\frac{i}{\epsilon}[\Phi_2^\star + \frac{1}{2}\Phi''_{2\star}(\beta_1-\beta^\star)^2 + \frac{1}{6}\Phi'''_{2\star}(\beta_1-\beta^\star)^3]} d\beta_1, \tag{45}$$

where we omit to indicate all the independent variables to simplify notations. The range of validity of this expression is in a neighbourhood of the the saddle point defined by $\Phi'_{2\star} = 0$. The integral (45) can be reduced, by a suitable rescaling of the integration variable, to a Airy function defined as follows:

$$Ai(Z) = \frac{1}{2\pi i}\int_{\infty e^{-i\pi/3}}^{\infty e^{+i\pi/3}} e^{\frac{t^3}{3} - Zt} dt. \tag{46}$$

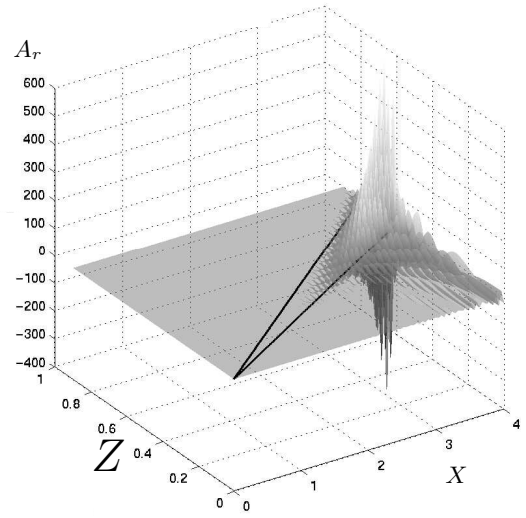

FIG. 9: Wedge-shaped disturbance in a parallel Blasius flow at $Re = 1000, \omega = 0.025$.

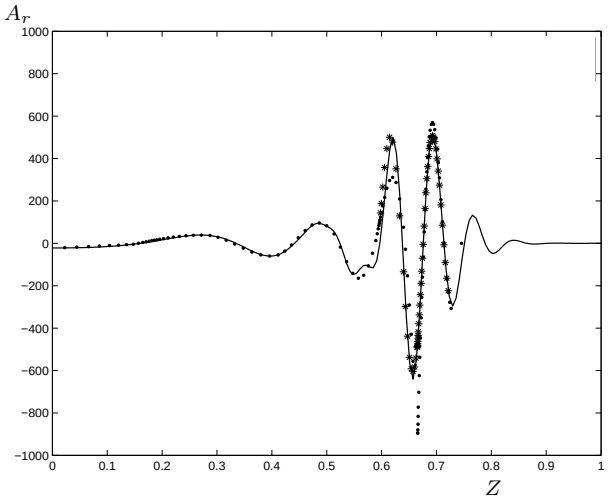

FIG. 10: Comparison of direct computation of the integral and ray theory for the parallel Blasius flow at $Re = 1000, \omega = 0.025$ and $X = 4$. (–) direct computation of the integral, (.) first order steepest descent, (*) second order correction.

It results that:

$$\mathbf{a}_{int}(X_2, Z_2, Y) \simeq \mathcal{A}(X_2, Z_2, \beta^\star)\hat{\mathbf{a}}_0(X_2, Z_2, X_1, \beta^\star, Y)\times \frac{2\pi i}{R} e^{i\frac{1}{\epsilon}(\Phi_{2\star} + \frac{(\Phi''_{2\star})^3}{3(\Phi'''_{2\star})^2})} Ai\left(\frac{i\frac{1}{\epsilon}(\Phi''_{2\star})^2}{2\Phi'''_{2\star}R}\right), \tag{47}$$

with R defined as follows:

$$R = \sqrt[3]{\frac{\frac{1}{\epsilon} i\Phi'''_{2\star}}{2}}. \tag{48}$$

R being a multi-valued cubic root, its choice depends on

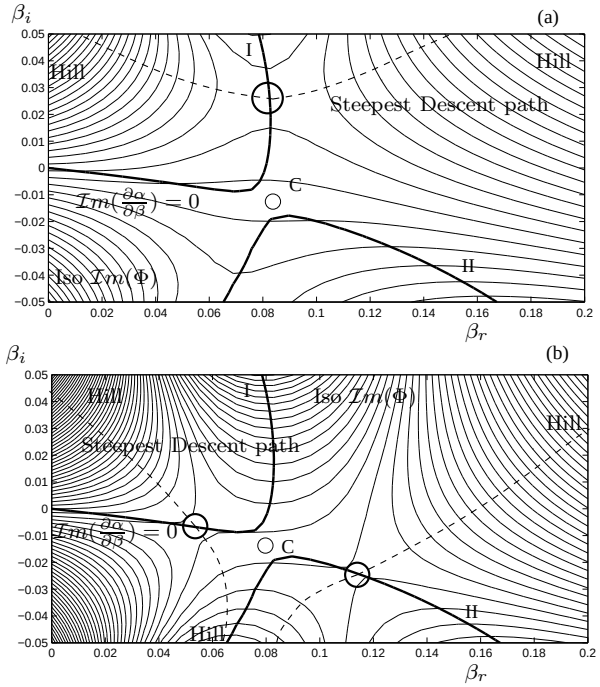

FIG. 11: Steepest descent path for a Blasius flow with $Re = 1000 and \omega = 0.025$, for the ray $\frac{Z}{X} = 0.2$ (a) and $\frac{Z}{X} = 0.15$ (b). The locus of the saddle points of real group direction is composed by two branches, I and II, shown with thick lines. The steepest descent paths can present one (a) or two (b) saddle points. In this latter case one must verify the relative importance of the two contributions. At a caustic, *i.e.* when branches I and II join, the approximation of ray theory is invalid and an approximation based the Airy functions must be employed.

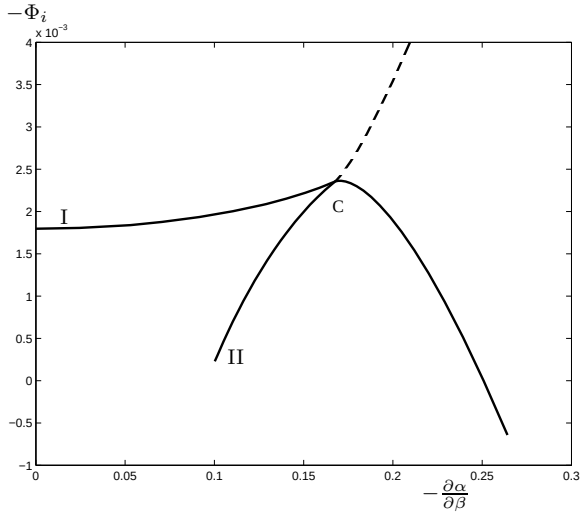

FIG. 12: Amplification rate $(-\Phi_i)$ as function of the group direction along the branch I and II (see figure 11) where the group direction is real for a Blasius flow, $Re = 1000, \omega = 0.025$ close to a caustic. Branch II is dotted when the steepest descent path does not have a saddle point on it, i.e. branch II no longer brings a contribution to the disturbance.

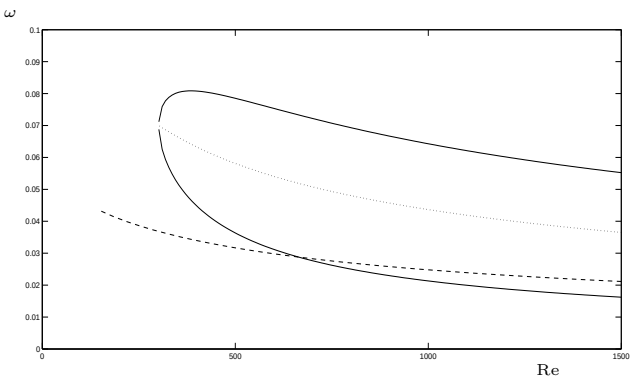

FIG. 13: Solid line: parallel neutral curve for the Blasius boundary layer. The curve of caustics (- -) is plotted and is found to lie close to the lower neutral branch. Dots are used to show the locus of the points of maximum amplification.

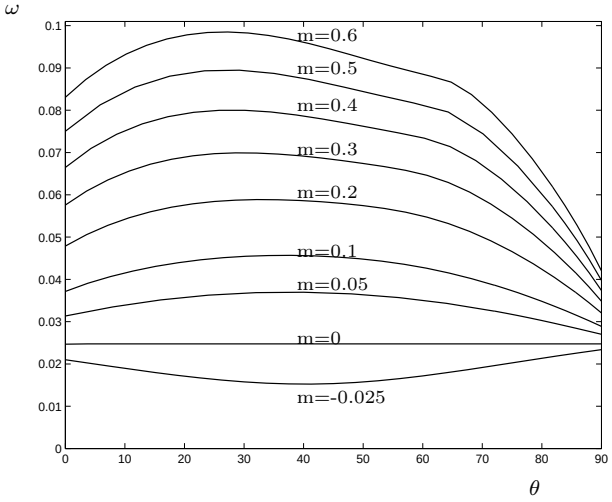

FIG. 14: Location of caustic points for different pressure gradients at $Re = 1000$.

the initial configuration of the steepest-descent contour.

The above result (the "Airy approximation", see [39]) is shown with the thin-dot curve in figure 8, and as the curve labelled "second order correction" in figure 10, which corresponds to the near singular case of figure 11b. The results are satisfactory in all cases.

C. Spatial localization of caustics

Having established the existence of caustics in boundary layers, it would be of interest to determine whether they have an influence on transition. In fact, when caustics are present ray methods predict infinite disturbance amplitudes and fail, unless the correction (47) is applied. For these reasons, it is interesting to locate caustics in the $(\alpha, \beta, \omega, Re)$ space to see whether they can be found next to the most amplified modes. Figure 13 shows the neutral curve for two-dimensional disturbances together with the locus of the caustics in the frequency-Reynolds number plane for a Blasius flow. The caustics cross into the unstable zone close to $Re = 650$, but remain rather close to the lower branch of the neutral curve. Since the most amplified modes are approximately centred between the two neutral branches (*cf.* dotted line in the figure), one can conclude that caustics should not hold a relevant role in the two-dimensional case in triggering transition to turbulence.

The situation is different, however, for the Falkner-Skan-Cooke flow, where two parameters can be independently varied, the sweep angle θ and the pressure gradient (defined through the parameter m). Table 1 provides the location of caustic points as function of different variables for selected combinations of angle and pressure gradient.

At a Reynolds number of 1000, figure 14 shows the frequencies at which caustics occur. This figure brings out the role of the pressure gradient on the caustics: the larger the pressure gradient, the larger the frequency at which caustics appear. The dependence with the sweep angle is not monotonic: for positive pressure gradients, the frequency of caustics presents a peak (around 20-30 degrees), which turns into a minimum when the pressure gradient becomes adverse.

Figure 15 displays the curves of caustic points at $Re = 1000$ together with the line joining the points of maximum amplification, as a function of θ and for some representative values of m. It appears that when the sweep angle is large (typically beyond 70 degrees), caustics can be found in conditions for which the spatial amplification is maximum (or near maximum), thus implying the potential for very large amplification. In such circumstances where the caustic curve "touches" the line of maximum amplification, particular care should be paid when computing the amplification rates of the instability.

V. NON-PARALLEL FLOWS

In the previous sections, ray theory has been validated on parallel flow configurations and its accuracy has been demonstrated; we can now test the method on non-parallel cases. This constitutes indeed the real interest of the method, since the dependence on the X-direction is no longer sinusoidal, and the "exact" integration of the disturbance wave packet employed earlier to verify ray theory results can no longer be applied.

A. Example

We choose here to illustrate by way of an example some of the conclusions drawn in the previous part. We take a Falkner-Skan-Cooke similarity solution at $X_1 = 1$, char-

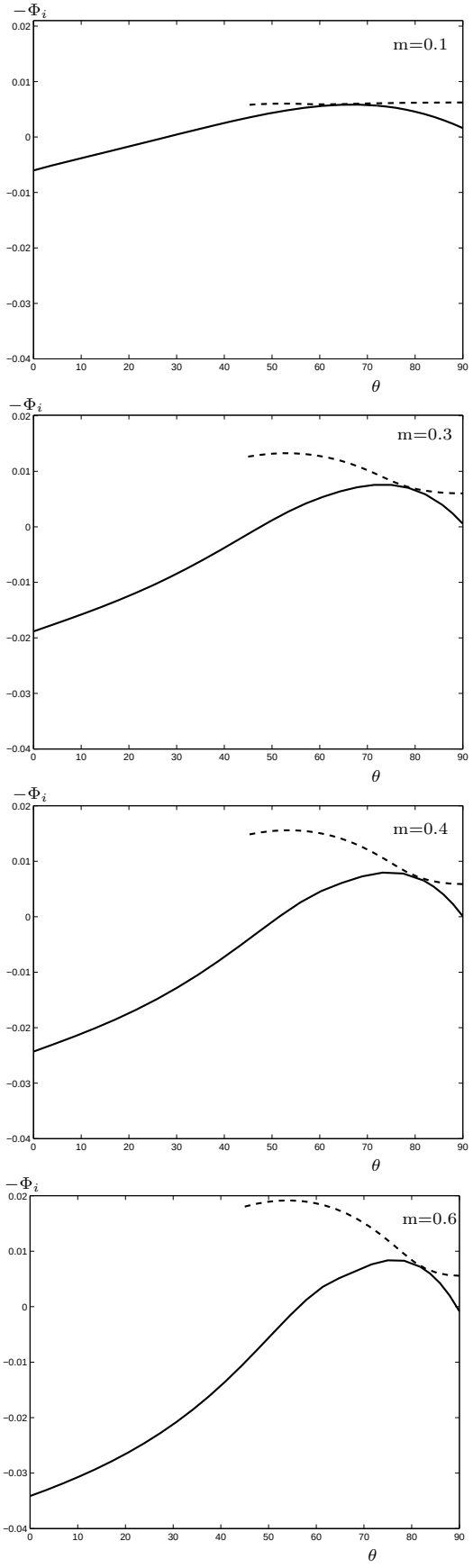

FIG. 15: Amplification rate as a function of the angle θ at $Re = 1000$ for different pressure gradients. Curve of caustic points (—) and of maximum amplification rate (- - -). For each value of m, the sweep angle where the two curves are tangent (or appear to intersect) is that for which the presence of caustics should be most relevant for transition.

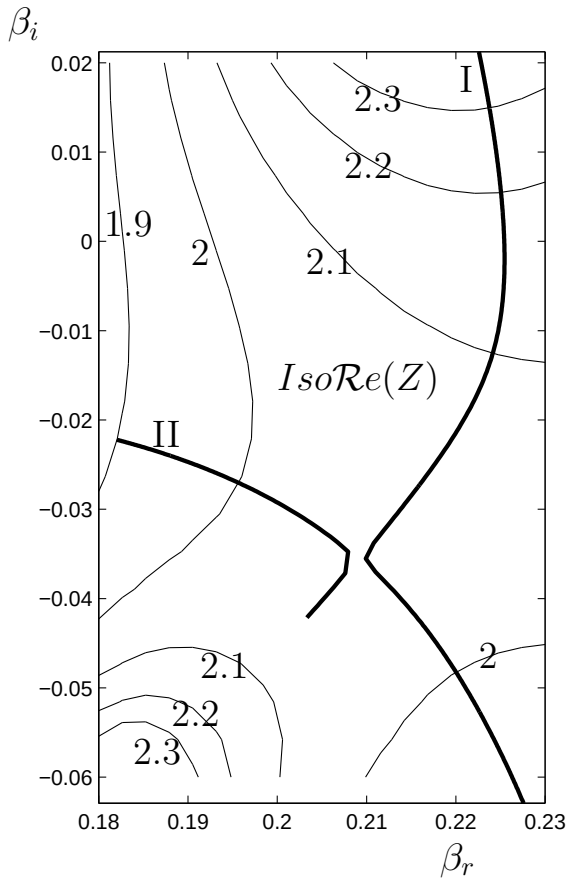

FIG. 16: Caustic in a non-parallel Falkner-Skan-Cooke flow with $\theta = \pi/3$, $m = 0.3$, $Re = 800$, $\omega = 0.0607$ at $X_2 = 2$. Branches I and II represent the locus of points in the β plane for which the final Z point is real.

acterized by $Re = 800$, $m = 0.3$ and with a yaw angle $\theta = \pi/3$, and let it evolve (grow) in the streamwise direction. We further suppose that a harmonic pointwise disturbance of frequency $\omega = 0.0607$ is applied at X_1 (with the initial value of Z arbitrarily fixed at 0) and evolves in space, simultaneously spreading along the span. As the equations are marched downstream, along the rays, the parameters of the adimensionalisation are maintained constant, *i.e.* those of the inflow position. Under these conditions a caustic appears at $X_2 = 2$.

As in the parallel case, we can find the locus of saddle points in the β-plane. Figure 16 shows the curves over which the final position Z is real, which is the analogue of having a real group direction d_g in the parallel case. Just like in the parallel case, the property that the maximum amplification is found for real β_1 holds (indeed, equation (43) applies in general and when the mean flow in the Z-direction is homogeneous $\beta_2 = \beta_1$.)

Figure 16 also displays two branches of real Z_2 pinching at the caustic. It is therefore interesting to understand how this can affect the estimate of the instability growth. For a given real Z_2, two rays from branch I and II arrive

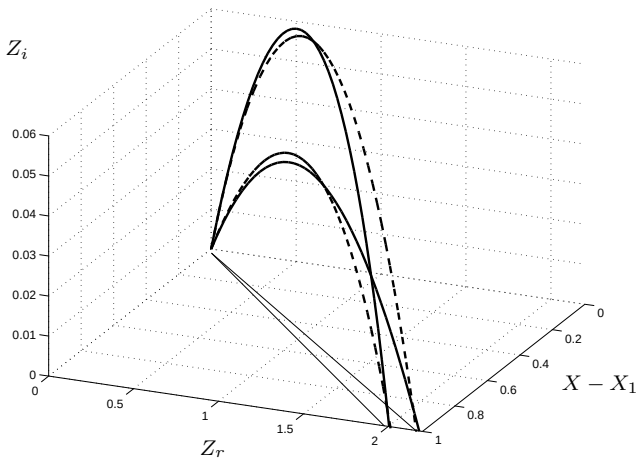

FIG. 17: Ray trajectories in the complex plane ($X-X_1$,Z_r,Z_i) for a non parallel Falkner-Skan-Cooke flow with $\theta = \pi/3$, $m = 0.3$, $Re = 800$, $\omega = 0.0607$. (—) corresponds to rays on branch I and (- - -) to rays on branch II.

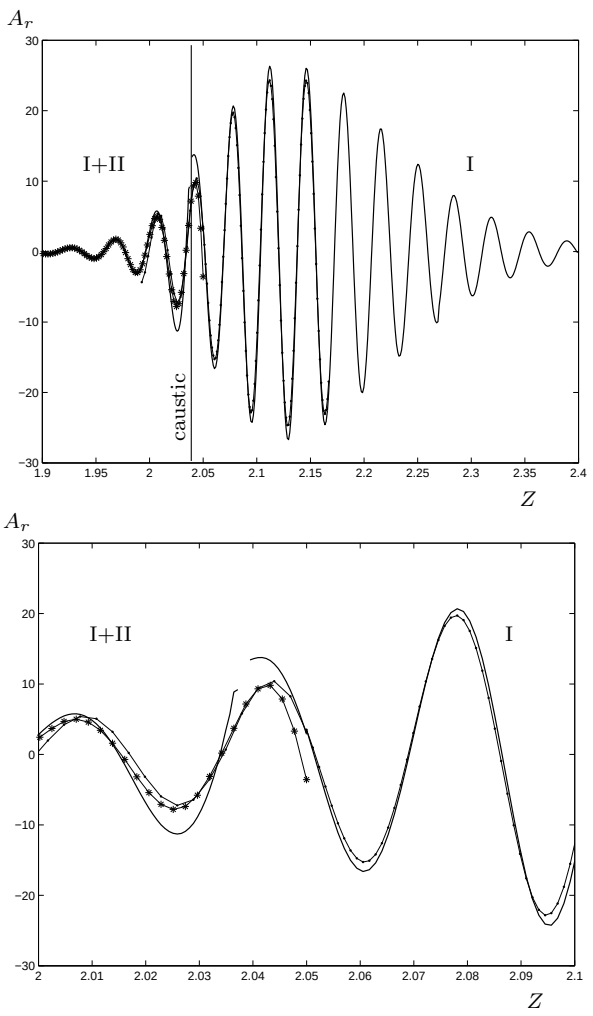

FIG. 18: Treatment of a caustic in a non-parallel Falkner-Skan-Cooke flow with $\theta = \pi/3$, $m = 0.3$, $Re = 800$, X=2, $\omega = 0.0607$. Different approximations for $\mathcal{R}e(A)$ function of the chordwise direction Z. A caustic is situated at $Z_{caus} = 2.037$. The first order geometrical optics approximation (—) is given by branch I for $Z > Z_{caus}$ and from the sum of the contributions of branches I and II for $Z < Z_{caus}$. The dotted line (...) is the approximation with Airy functions from branch I, valid for $Z > Z_{caus}$. The stars denote the Airy approximation resulting from the contributions of branches I and II, valid for $Z < Z_{caus}$.

at this downstream location as illustrated in figure 17; they have been computed by solving equation (35) iteratively.

We observe that the ray which has the larger maximum in the complex Z-plane has the smaller amplification rate. At a caustic these two rays become tangent, a condition expressed by $\frac{\partial^2 \Phi_2}{\partial \beta_1^2} = 0$. The location of the caustic in the final plane is $Z_{caus} = 2.037$ for this case. To know which rays have to be taken into account to evaluate the wave amplitude, we should look at the steepest descent path in figure 16. The configuration is analogous to that of the parallel case studied earlier on. If $Z_2 > Z_{caus}$, the saddle points are present only on branch I. On the contrary, if $Z_2 < Z_{caus}$ two branches, I and II, provide saddle points which may contribute to the integral. The first order ray approximation is derived from equation (36); for $Z_2 < Z_{caus}$ the two saddle point contributions must be added to one another. Results for the real part and absolute value of the disturbance amplitude A at $X_2 = 2$ are given in figures 18 and 19. When the first order approximation is close to Z_{caus} the term $\Phi_2^{''}$ in equation (2.36) approaches zero causing divergence of the result. To achieve a continuous approximation of the disturbance, locally valid around the caustic, the Airy approximation (4.3) must be used.

As for the first order ray approximation, the Airy expansion is derived on each branch, the final amplitude is obtained by summing the two contributions for $Z_2 < Z_{caus}$ whereas, for $Z_2 > Z_{caus}$ only branch I counts. As displayed in figure 18 (b), the Airy approximations (on both sides of Z_{caus}) match one another in correspondance of the caustic. Continuity is ensured at $Z = Z_{caus}$, the point where the two branches pinch, but special care must be paid at choosing the correct value of R when going through the singularity (*cf.* equation 48).

The difference in results that can be observed in figure 18 between the first order ray approximation of the disturbance amplitude and Airy approximation reflects the limitations of the steepest descent methode close to caustics.

With the approximation through Airy functions, we thus possess a tool to properly compute instabilities in non-parallel flows, even when ordinary ray theory diverges.

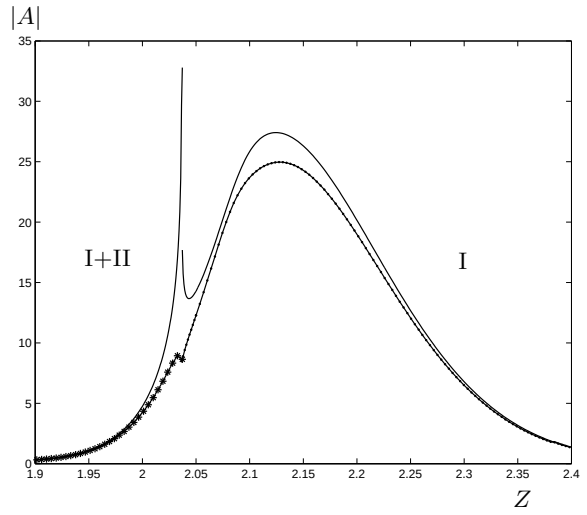

FIG. 19: Different approximations for $|A|$ along the chord Z. Parameters and symbols as in figure 18.

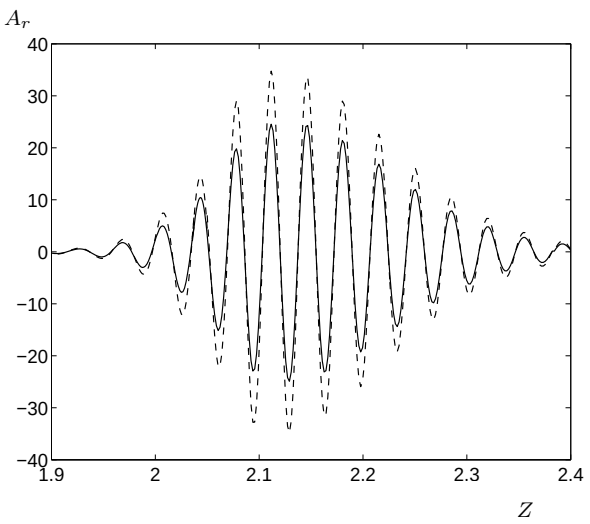

FIG. 20: Non parallel Falkner-Skan-Cooke flow with $\theta = \pi/3$, $Re = 800$, X=2, $\omega = 0.0607$. Comparison between geometrical optics (—) and physical optics (- - -) for the Airy approximation.

B. Physical optics

We have also implemented the physical-optics approximation, as described in section (2.8)[41].

In the physical-optics approximation, for a given frequency, the amplification factor of the unstable disturbance wave at the position X_2 is defined as:

$$\int_{X_1}^{X_2} \left(-\frac{1}{\epsilon}\alpha_i + \left(\frac{< \hat{\mathbf{b}}_0, \gamma_\mathbf{0} >}{< \hat{\mathbf{b}}_0, \gamma_\mathbf{X} >} \right)_r \right) dX, \qquad (49)$$

with the path of integration taken along the rays. The results for the growth rate depend on the normalization chosen for the eigenfunctions, and here we have imposed that the maximum of $\hat{v}$ equals 1.

An application to the Falkner-Skan-Cooke flow is shown in figure 20, for both geometrical and physical optics with the Airy approximations. Although the wave packet computed with the higher order approximation is in phase (along Z) with that arising from the geometrical optics, the amplification undergone by the wave is quite different, an indirect indication of the effect of baseflow non-parallelism. In both cases the curves are very smooth, an indication of the correct handling of singularities.

VI. DISCUSSION AND CONCLUDING REMARKS

The method of ray theory up to the physical-optics approximation has been presented here in details starting from the Navier-Stokes equations. After representing the disturbance with a WKB ansatz, the eikonal equation for the problem is obtained in the form of a dispersion relation tying the first derivatives of the phase (which can be interpreted as a local wavenumber and frequency). This equation is solved by the method of characteristics, leading to the equation of rays. As the dispersion relation is complex the characteristics are too (except for the trivial case of neutral disturbances in a parallel flow for which rays are straight lines in the $X - Z$ plane) entailing an analytic extension of all dependent variables for complex values of the spatial coordinates. The ray trajectories, phase and amplitude propagation are therefore computed using the local eigenvalue problem. The disturbance at a given final location can be written in the form of a Maslov integral as the sum of all rays passing through this point. A choice for the representation here has to be made. Rays can indeed be parameterized employing the initial spanwise position Z or the initial spanwise wavenumber β. A similar choice arises in classical mechanics where, for a set final position and time, we can parameterize the trajectory of a particle arriving at that point either by its initial position or its initial momentum. For a Dirac delta disturbance at a point in space the spatial representation has to be discarded, because it violates the assumption of slow spatial variation, and the representation in spectral space becomes compulsory. It is, however, possible to simplify this integral representation by using the steepest-descent method. Under the same assumptions that underlie the original WKB ansatz, it is sufficient to consider the saddle points giving the main contribution to the integral, and therefore we deform the contour of integration to pass through these points. The asymptotic method has been verified to provide an accurate approximation for reasonable values of the Reynolds number, and not only in the infinite limit.

In the example of a parallel flow without pressure gra-

dient, for a given forcing frequency, the approximation is good as long as the steepest-descent path presents one saddle point with a dominant amplification rate. This is not always the case for the present problem of harmonic forcing in time (as opposed to the situation of time-impulsive excitation considered by other authors). Indeed, the integral for the disturbance over the spanwise wavevector turns out to present two branches of saddle points. If both branches have an amplification rate of the same order, then two rays have to be taken into account to compute the instability. The limit case where these two branches pinch together corresponds to a caustic, where both the first and second derivative of the complex phase with respect to β equal zero. This does not occur in the case of time-impulsive forcing, studied by [1] and many authors thereafter ([37], [34]). These authors did not find any caustics because in their case the condition, $\Delta = \left[\left(\frac{\partial^2\omega}{\partial\beta\partial\alpha}\right)^2 - \frac{\partial^2\omega}{\partial\beta^2}\frac{\partial^2\omega}{\partial\alpha^2}\right]^{\frac{1}{2}} = 0$ does not occur. One way of understanding this is to make an analogy with the problem of harmonic versus impulsive excitation of surface waves in a water pool. In the harmonic case, the most prominent example of which is the ship wake generated when the frequency is zero but the water is moving (with respect to the ship, at least!), caustics arise from the interaction between two kinds of wave fronts. On the other hand, no caustics occur when a stone is dropped through the water (impulsive excitation).

As far as the distribution of caustics is concerned, in the Blasius boundary layer we found that the curve of caustics in the (ω, Re) plane is close to the lower neutral curve. In the case of a Falkner-Skan-Cooke flow, on the other hand, caustics also appear in the amplified zone, yielding a significant cumulative effect. A parametric study has been conducted for different sweep angles θ and pressure gradient (represented through the velocity exponent m). Under most conditions caustics are not situated close to the most amplified direction, but this does happen for large sweep angles. In a neighbourhood of caustics the combined effect of the two branches of the dispersion relation cannot be neglected, as has been shown through several examples. To take into account the correction to the growth rate due to the caustic singularity, we applied Airy asymptotic method obtained upon developing the phase in a Taylor series up to the third order around the saddle point. This correction, which is expressed in terms of Airy functions and has been derived here for the first time for boundary-layer instabilities, prevents the approximation from diverging at the caustic and also provides a much better approximation of the maximum amplification rate. Finally, an application to a non-parallel flow case has been illustrated.

VII. ACKNOWLEDGEMENTS

We are grateful to Dr. N. Itoh for several reprints of his papers on stability and complex-ray theory, to Prof. W.O Criminale for making available a copy of [16], and to Prof. H. Gustavsson for providing a copy of his Ph.D. thesis. The work is financially supported by the French Ministry of Defense through a Ph.D scholarship awarded to the first author.

APPENDIX A

$$
\begin{aligned}
A_1 &= -U_0u_{0X} - V_1u_{0Y} - W_0u_{0Z} - u_0U_{0X} - w_0U_{0Z} \\
&\quad -p_{0X} - v_0U_1 + \tfrac{2i}{Re}(\alpha u_{0X} + \beta u_{0Z}) \\
A_2 &= -U_0v_{0X} - V_1v_{0Y} - W_0v_{0Z} - v_0V_{1Y} - p_{0Y} \\
&\quad -i\alpha v_0U_1 - i\beta v_0W_1 + \tfrac{2i}{Re}(\alpha v_{0X} + \beta v_{0Z}) \\
A_3 &= -U_0w_{0X} - V_1w_{0Y} - W_0w_{0Z} - u_0W_{0X} - w_0W_{0Z} \\
&\quad -p_{0Z} - v_0W_1 + \tfrac{2i}{Re}(\alpha w_{0X} + \beta w_{0Z}) \\
A_4 &= -u_{0X} - w_{0Z}
\end{aligned}
\tag{A1}
$$

APPENDIX B

$$
\boldsymbol{\gamma_0} = -\begin{pmatrix}
(U_0 - \frac{2i\alpha}{Re})\hat{u}_{0X} + V_1\hat{u}_{0Y} + (W_0 - \frac{2i\beta}{Re})\hat{u}_{0Z} \\
+U_{0X}\hat{u}_0 + U_{0Z}\hat{w}_0 + \hat{p}_{0X} + \hat{v}_0U_1 \\
\\
(U_0 - \frac{2i\alpha}{Re})\hat{v}_{0X} + V_1\hat{v}_{0Y} + (W_0 - \frac{2i\beta}{Re})\hat{v}_{0Z} \\
+V_{1Y}\hat{v}_0 + \hat{p}_{0Y} + i\alpha\hat{v}_0U_1 + i\beta\hat{v}_0W_1 \\
\\
(U_0 - \frac{2i\alpha}{Re})\hat{w}_{0X} + V_1\hat{w}_{0Y} + (W_0 - \frac{2i\beta}{Re})\hat{w}_{0Z} \\
+W_{0X}\hat{u}_0 + W_{0Z}\hat{w}_0 + \hat{p}_{0Z} + \hat{v}_0W_1 \\
\\
\hat{u}_{0X} + \hat{w}_{0Z}
\end{pmatrix}
\tag{B1}
$$

$$
\boldsymbol{\gamma_X} = -\begin{pmatrix}
(U_0 - \frac{2i\alpha}{Re})\hat{u}_0 + \hat{p}_0 \\
(U_0 - \frac{2i\alpha}{Re})\hat{v}_0 \\
(U_0 - \frac{2i\alpha}{Re})\hat{w}_0 \\
\hat{u}_0
\end{pmatrix},\ \boldsymbol{\gamma_Z} = -\begin{pmatrix}
(W_0 - \frac{2i\beta}{Re})\hat{u}_0 \\
(W_0 - \frac{2i\beta}{Re})\hat{v}_0 \\
(W_0 - \frac{2i\beta}{Re})\hat{w}_0 + \hat{p}_0 \\
\hat{w}_0
\end{pmatrix}
\tag{B2}
$$

APPENDIX C: CHARACTERISTIC LINES FOR THE AMPLITUDE EQUATION

With a suitable choice of variables (in this case u, v, v_x, w, w_x, p), it is always possible to choose the state vector $\mathbf{a}$ for the stability equations so that the problem is recast as a system of first-order differential equations, of the form:

$$\epsilon\left(A\mathbf{a}_X + B\mathbf{a}_Z\right) = C\mathbf{a} \tag{C1}$$

where A, B, C are suitable 6×6 matrices. The disturbance is then expressed in the form of a WKB ansatz: $\mathbf{a} = e^{i\frac{\Phi}{\epsilon}}(\mathbf{a_0} + \epsilon\mathbf{a_1} + ...)$. By injecting into (C1) it is found that:

- Order ϵ^0:

$$i\alpha A\mathbf{a_0} + i\beta B\mathbf{a_0} = C\mathbf{a_0} \tag{C2}$$

- Order ϵ^1:

$$i\alpha A\mathbf{a_1} + i\beta B\mathbf{a_1} - C\mathbf{a_1} = -A\mathbf{a_0}_X - B\mathbf{a_0}_Z \tag{C3}$$

We express the zeroth-order solution as the product of a normalized eigenfunction and an amplitude: $\mathbf{a_0} = \mathcal{A}\hat{\mathbf{a}}_0$. The equation for the amplitude (28), given by the compatibility condition applied to the ϵ^1-order equation can be written as:

$$\begin{aligned} &< \hat{\mathbf{b}}_0, A\hat{\mathbf{a}}_0 > \mathcal{A}_X + < \hat{\mathbf{b}}_0, B\hat{\mathbf{a}}_0 > \mathcal{A}_Z = \\ &-\mathcal{A}\left(< \hat{\mathbf{b}}_0, A\hat{\mathbf{a}}_{0X} > + < \hat{\mathbf{b}}, B\hat{\mathbf{a}}_{0Z} >\right), \end{aligned} \tag{C4}$$

where $\hat{\mathbf{b}}_0$ is the normalized left eigenvector, solution of the adjoint problem. We now prove that the characteristic direction for equation (C4), *i.e* $\frac{dZ}{dX} = \frac{<\hat{\mathbf{b}}_0, A\hat{\mathbf{a}}_0>}{<\mathbf{b}_0, B\hat{\mathbf{a}}_0>}$ is given by $-\frac{\partial\alpha}{\partial\beta}$ just as the characteristic direction of equation (C2). For this purpose we differentiate (C2) with respect to β to get:

$$i\left(A\frac{\partial\alpha}{\partial\beta} + B\right)\hat{\mathbf{a}}_0 = (C - A\alpha - B\beta)\frac{\partial\hat{\mathbf{a}}_0}{\partial\beta} \tag{C5}$$

Upon taking the scalar product of (C5) with the left eigenvector, the right-hand side vanishes and we obtain the result required. Therefore, even when the dispersion relation is complex, the amplitude equation has the same rays as the eikonal equation.

[1] M. Gaster, J. Fluid Mech., **32**, 173 (1968).
[2] M. T. Landahl, J. Fluid Mech., **56**, 775 (1972).
[3] W.D. Hayes, Proc. R. Soc. London Ser. A., **26**, 320 (1970).
[4] G.B. Whitham, *Linear and Nonlinear Waves.* John Wiley and Sons, New York, 1974.
[5] N. Itoh, N. *Proceedings IUTAM Symposium on Laminar-Turbulent Transition*, Edited by R.Eppler and H.Fasel, Springer, Berlin, 1980.
[6] M. Gaster, Proc. Soc. Lond., **384**, 317 (1982).
[7] L. Brevdo, Z. Angew. Math. Phys., **42**, 911 (1991).
[8] M. Gaster, J. Fluid Mech., **121**, 365 (1982).
[9] T. Cebeci and K. Stewartson AIAA paper 79-0263, New Orleans,La, 1979.
[10] N. Itoh, Fluid. Dyn. Research., **18**, 337 (1996).
[11] R.J. Lingwood, Eur. J. .Mech. B/Fluid., **18**, 581 (1999).
[12] S.J. Chapman, J.M.H Lawry, J.R. Ockendon and R.H. Tew SIAM Review., **41**, 417 (1999).
[13] Yu, A. Kravtsov,G.W. Forbes and A.A. Asatryan, *Theory and Application of Complex Rays.* Progress in Optics Series, **39**, Elsevier, Amsterdam,1999.
[14] J. Lighthill, *Waves in Fluids.* Cambridge Mathematical Library,1978.
[15] A. Gustavsson, 1978 *On the evolution of disturbances in boundary layer flows.* Ph.D. thesis, Royal Institute of Technology, Stockholm, Sweden, 1978.
[16] M. Gaster, *On the application of ray mathematics to non conservative systems.* Geofluid Dynamical Wave Mathematics, Applied Mathematics Group, University of Washington, Seattle, 1978.
[17] M. Bouthier, J. de Mécanique., **11**, 599 (1972).
[18] M. Gaster, J. Fluid Mech., **66**, 465 (1974).
[19] W.S. Saric and A.H. Nayfeh, Phys. Fluids., **18**, 945 (1974).
[20] N. Itoh, Fluid. Dyn. Research., **1**, 119 (1986).
[21] J. Cousteix and J. Mauss, *Analyse Asymptotique et Couche Limite.* In press, 2005.
[22] R. Govindarajan and R. Narasimha, J. Fluid Mech., **439**, 403 (2001).
[23] F. Giannetti and P. Luchini, *Leading edge receptivity by adjoint methods.* Submitted to *J. Fluid Mech.*, 2004
[24] R. Courant and D. Hilbert *Methods for Mathematical Physics.* Vol 2, Interscience, 1962.
[25] L. Landau and E. Lifchitz, *Mécanique.* Cours de physique théorique. MIR, Moscou, 1964.
[26] D.C. Hill, J. Fluid Mech., **292**, 183 (1995).
[27] P. Luchini and A. Bottaro, Phys. Fluids., **13**, 1668 (2001).
[28] P. De Matteis, R.S. Donelli and P. Luchini, *Application of the ray-tracing theory to the stability analysis of three-dimensional incompressible boundary layers.* XIII AIDAA Conference, Rome, 1995.
[29] M.G. Brown, Wave Motion, **32**, 247 (2000) The Maslov integral representation of slowly varying dispersive wavetrains in inhomogeneous moving media.
[30] C.M. Bender and S.A.Orzag *Advanced Mathematical Methods for Scientists and Engineers.* McGraw-Hill, New York, 1978.
[31] J.C. Cooke, Proc. Camb. Phil. Soc., **46**, 645 (1950).
[32] H. Schlichting, *Boundary-Layer Theory.* Seventh edition, McGraw-Hill, New-York,1978.
[33] R.J. Briggs, *Electron-Stream Interaction with Plasmas.* MIT press, Chap 2, 1964.
[34] R.J. Lingwood, Stud. Appl. Math, **98**, 213 (1997).
[35] R.J. Lingwood, J. Fluid. Mech., **344**, 317 (1997).
[36] Yu. A. Kravtsov and Y. Orlov, *Caustics, Catastrophes, and Wave Fields.* Springer-Verlag, New York, 1999.
[37] M. Taylor and N. Peake, J. Fluid. Mech., **355**, 359 (1998).
[38] J.J. Healey, J. Fluid. Mech., **511**, 179 (2004).
[39] C. Chester, B. Friedman and F. Ursell, Proc. Cambridge Phyl. Soc., **53**, 599 (1957).
[40] Sometimes the so-called *real axis-approximation* is adopted, consisting in keeping β real and neglecting the

imaginary part of $\frac{\partial \alpha}{\partial \beta}$. This is equivalent to using the stationary-phase rather than the saddle-point approximation of the integral (32), and quickly becomes inaccurate when the complex saddle point $\beta^\star$ is far from the real axis.

[41] The base flow terms U_1 and W_1 are not included in the approximation.

Re	m	θ (deg.)	ω	$\beta^\star$	$\alpha^\star$	$\frac{\partial\alpha}{\partial\beta}^\star$
1000	0	0	0.0247	0.0796 - 0.0125i	0.0763 - 0.0001i	-0.1676
	-0.025	0	0.0210	0.0700 - 0.0130i	0.0668 - 0.0024i	-0.1695
		60	0.0172	0.0616 - 0.0042i	0.0563 + 0.0016i	-0.1834
	0.3	0	0.0576	0.1596 - 0.0054i	0.1555 + 0.0197i	-0.1592
		60	0.06491	0.2377 - 0.0371i	-0.05494 + 0.0742i	-0.2354
500	0	0	0.0317	0.0912 - 0.01063i	0.0871 + 0.0028i	-0.1666

TABLE I: Values of the different parameters on some representative caustics. Superscript * denotes that the variable is evaluated at the saddle point.